Boundary-Layer Meteorol
DOI 10.1007/s10546-011-9682-5

ARTICLE

The Effect of the Screen on the Mass, Momentum, and Energy Exchange Rates of a Uniform Crop Situated in an Extensive Screenhouse

Mario B. Siqueira · Gabriel G. Katul · Josef Tanny

Received: 31 May 2011 / Accepted: 28 November 2011

Abstract The area of crops cultivated in extensive screenhouses is rapidly growing, especially in semi-arid and arid regions. Water vapour, carbon dioxide, and sensible heat released or taken up by crops within such protected environments can substantially alter the immediate micro-environment, which in turn, affects these fluxes. This amplified interaction between plants and their microclimate challenges simple assessments on how partially covering the crop by a screen modifies plant water uptake and photosynthesis. Via a newly proposed higher-order closure model, the effects of a screen on the mean flow field, turbulent stresses, radiative and energy fluxes, as well as scalar sources, sinks, fluxes, and mean scalar concentration within screenhouses are explored. As a starting point, an extensive screenhouse is assumed thereby reducing the sensitivity of the model results to the precise geometric configuration of the screenhouse. The model findings for the screenhouse are presented and referenced against their open field counterpart. The radiation modulation and changes to turbulent transport due to the presence of the screen are investigated. In general, the presence of a screen results in a warmer and more humid environment inside the screenhouse, promoting reductions in both canopy photosynthesis and transpiration. However, the overall effect of

M. B. Siqueira (✉)
Department of Mechanical Engineering, Universidade de Brasilia, Brasilia, Brazil
e-mail: mariosiqueira@unb.br

G. G. Katul
Nicholas School of the Environment, Duke University, Durham, NC, USA
e-mail: gaby@duke.edu

G. G. Katul
Department of Civil and Environmental Engineering, Pratt School of Engineering,
Duke University, Durham, NC, USA

J. Tanny
Institute of Soil, Water and Environmental Sciences, Agricultural Research Organization,
Volcani Center, Bet Dagan, Israel
e-mail: tanai@volcani.agri.gov.il

Published online: 24 December 2011

the screen is to enhance water-use efficiency thereby resulting in water savings for the same amount of gross primary production.

Keywords Banana crop · Canopy turbulence · Carbon dioxide uptake · Evapotranspiration · Higher-order closure modelling · Radiation attenuation · Screenhouse · Water-use efficiency

List of Symbols

A	Leaf area density
$a_1,\ a_2$	Constants for V_{cmax} temperature correction
A_{n}	Leaf-level net photosythesis
b	Residual stomatal conductance
c	Generic scalar
$c_1,\ c_2,\ c_1'$	Turbulence model empirical constants (stress equation)
$C_{\mathrm{a,can}}$	Mean canopy air CO_2 concentration
C_{d}	Drag coefficient for the leaves
$C_{\mathrm{d,sc}}$	Drag coefficient for the screen
$C_{\mathrm{L,can}}$	Leaf intercellular CO_2 concentration
C_{L}	Mean canopy leaf internal CO_2 concentration
C_{leaf}	Leaf specific heat
C_{oa}	Oxygen concentration in air
C_{s}	CO_2 concentration at leaf surface
$c_{\mathrm{s}},\ c_{\theta 3}$	Turbulence model constant (fluxes)
c_{sc}	Screen specific heat
$c_{\varepsilon 1},\ c_{\varepsilon 2},\ c_{\varepsilon 3}$	Turbulence model constants (dissipation equation)
D_0	Empirical coefficient
$D_{\mathrm{a,can}}$	Mean canopy-air vapour pressure deficit
D_{s}	Vapour pressure deficit at leaf surface
E	Screen-material emissivity
e_{m}	Maximum quantum efficiency
$F_{\mathrm{d,c}}$	Drag force by leaves
F_{c}	CO_2 flux
G	Leaf conductance
g_{bl}	Leaf boundary-layer conductance
$g_{\mathrm{s,c}}$	Stomatal conductance
g_{sc}	Screen boundary-layer conductance
I_{p}	Incident photosynthetically active radiation
k	Turbulent shear kinetic energy
$K_{\mathrm{C}},\ K_{\mathrm{O}}$	Michaelis–Menten constants
l_{bl}	Characteristic leaf dimension
L_{v}	Latent heat of vaporization of water
LW	Longwave radiation reaching canopy top
LW_{can}	Longwave radiation outgoing from the canopy volume
$LW_{\mathrm{in,o}}$	Incoming longwave over the screen (experiment)
$LW_{\mathrm{in,u}}$	Incoming longwave under the screen (experiment)
$LW_{\mathrm{out,o}}$	Outgoing longwave over the screen (experiment)
$LW_{\mathrm{out,u}}$	Outgoing longwave under the screen (experiment)
LW_{sky}	Incoming atmospheric radiation

m	Physiological constant
m_{L}	Leaf mass
N	Prandtl number or Schmidt number
n_k	Unit vector normal to direction k
P	Production term (turbulence model)
R	Redistribution term (turbulence model)
R_{d}	Dark respiration
Re	Reynolds number
R_{N}	Net radiation
S_c	Local source/sink of scalar c
SH	Sensible heat flux
LH	Latent heat flux
S_{M}	Leaf latent heat source
S_{sc}	Local source/sink of sensible heat due to the screen
S_T	Leaf sensible heat source
SW_{b}	Direct beam solar radiation reaching canopy top
SW_{d}	Diffuse solar radiation reaching canopy top
$SW_{\mathrm{in,o}}$	Incoming shortwave over the screen (experiment)
$SW_{\mathrm{in,u}}$	Incoming shortwave under the screen (experiment)
$SW_{\mathrm{out,o}}$	Outgoing shortwave over the screen (experiment)
$SW_{\mathrm{out,u}}$	Outgoing shortwave under the screen (experiment)
$SW_{\mathrm{sun,b}}$	Incoming direct beam solar radiation
$SW_{\mathrm{sun,d}}$	Incoming diffuse beam solar radiation
t	Time
T	Transport term (turbulence model)
T_{L}	Leaf temperature
T_{sc}	Screen temperature
u	Streamwise velocity component (without subscript) or orthogonal velocity components (with subscript)
V_{cmax}	Maximum catalytic capacity of Rubisco per unit leaf area
$V_{\mathrm{cmax,25}}$	Maximum catalytic capacity of Rubisco per unit leaf area at 25°C
w	Vertical velocity component
z	Vertical coordinate

Greek Symbols

Γ^*	CO_2 compensation point
χ_c	Molecular diffusivity of generic scalar in air
α_{p}	Leaf absorptivity for photosynthetically active radiation
ε	Dissipation term (with subscript) or viscous dissipation rate (without subscript)
ϕ	Screen solidity
ε_c	SKE to WKE transformation
κ_1	Photosynthesis rate
κ_2	CO_2 concentration parameter (photosynthesis model)
ρ	Air density
σ_{SB}	Stefan–Boltzmann constant
$\rho_{\mathrm{sc,SW}}$	Screen-material reflectivity
$\tau_{\mathrm{SW,b}}$	Screen-material transmissivity to direct beam solar radiation

$\tau_{SW,d}$ Screen-material transmissivity to diffuse solar radiation
τ_t CO_2/O_2 specific ratio

1 Introduction

According to the Food and Agricultural Organization, agriculture consumes some 70% of the global water use (FAO 2011) and current projections suggest that this fraction will not decrease in the foreseeable future. Moreover, driven by food security and quality needs, agriculture is now increasingly situated within large-scale protected environments such as greenhouses and screenhouses. Compared to their 'open-field' counterparts, these protected environments offer a number of advantages such as reduced bird or insect invasions, reduced wind and hail damage, reduced radiative load and potential irrigation water saving (Tanny et al. 2006, 2010).

The water vapour, carbon dioxide, and sensible heat sources and sinks, and consequently the fluxes to and from crops within such a *partially* enclosed area, can substantially alter their micro-environment, which, in turn, affects these fluxes on short time scales. It is precisely this 'intensified' interaction between plants and their microclimate in protected environments, due to confinement promoted by the presence of the screen, that poses one of the main scientific challenges and is the primary thrust of our work. Another scientific challenge is that of crop acclimatization to this altered microclimatic state that leads to basic modifications in crop physiological attributes and carbon allocation patterns, which in turn, alters crop yield and quality. This acclimatization occurs on time scales commensurate with crop development, and hence, is significant on time scales much longer than the diurnal cycle. Addressing simultaneously these two challenges is well beyond the scope of a single study. Given that any progress on the second issue requires basic progress on the first, a logical starting point here is the intensified two-way coupling between plants and their microclimate. This is also receiving a broader interest within the ecological and climate sciences given the increased usage of growth chambers intended to investigate ecosystem responses to altered climatic conditions representing future climate scenarios (Fay et al. 2009; Manzoni et al. 2011).

The scope of our work is to assess how the intensification of the two-way coupling between plants and their microclimate in protected environments arises due to the presence of a porous screen covering the crop. A novel model is developed and simulations are conducted for a soil-plant system positioned in 'open' and 'screened' settings. The soil-plant systems in both settings have identical soil, physiological, drag, radiative, thermal, and aerodynamic properties. Both systems are forced by the same meteorological drivers specified well above the screen height. The model runs are then used to explore two inter-related questions: (i) how the presence of a screen alters the mean flow field, turbulent stresses, radiative and energy fluxes, as well as scalar sources, sinks, fluxes, and mean concentration, and (ii) to what extent the modifications in scalar sources, sinks, and fluxes are induced by the screen modifications to the radiation-energy balance versus the aerodynamic effects.

Models describing the energy, water vapour and CO_2 balances of greenhouse systems have been used to characterize micro-environmental conditions and to improve greenhouse design (Soribe and Curry 1973; Kindelan 1980; Yang et al. 1990; Boulard and Baille 1993; Boulard et al. 2002; Roy et al. 2002; Willits 2003; Singh et al. 2006; Majdoubi et al. 2009; Teitel et al. 2010). Most of these models generally neglect or oversimplify photosynthesis and transpiration, thus neglecting one of the key alterations induced by the vegetation to the canopy microclimate. On the other hand, canopy models that incorporate physiological,

radiative, and turbulent transport descriptions of vegetation-atmosphere interactions in open systems are becoming available and have been tested extensively using FluxNet datasets (Baldocchi and Meyers 1998; Lai et al. 2002; Tuzet et al. 2003; Daly et al. 2004; Siqueira et al. 2006; Juang et al. 2008). These canopy models can be extended to resolve both vegetation and atmospheric contributions to the coupled energy and mass fluxes in partially closed systems provided key modifications are implemented.

Here, a general soil-vegetation-atmosphere model applicable for both open and protected canopies is proposed. To address the two questions framing the scope of our work, two major advances in this type of model formulation are developed: (i) the inclusion of the screen effects on the flow field, which are introduced as a non-isotropic drag force whose effects are then propagated to the bulk mean flow, the entire turbulent stress tensor, and the mean turbulent kinetic energy (TKE) dissipation rate distribution, (ii) the inclusion of the screen effect on the heat, energy, and radiation budget components. As such, the model is able to resolve processes on time scales relevant to leaf, screen and soil (short time scales). Even though the time scale relevant to soil might be longer than those for the former two, the unsteady form of the evolution equations for leaf and screen is kept given that a non-steady state solution is required for the soil anyway. Again, it is not the intent here to investigate processes on time scales much longer than daily, such as growth or acclimatization.

2 Theory

In a spatially extensive screenhouse, the external flow traversing the screenhouse experiences a pressure drop due to the presence of screened side walls perpendicular to the mean wind direction. This pressure drop leads to a deceleration via advective terms as the flow adjusts to the canopy-soil system within the screenhouse until the advective terms themselves become negligible at some distance from the screened walls. Following this adjustment phase, the flow can then be considered 'in equilibrium' with the vegetated surface within the screenhouse. For this equilibrium state, all longitudinal and transversal gradients can be assumed negligible compared with their vertical counterparts.

Naturally, this assumption is appropriate only for extensive screenhouses enclosing a uniform canopy in which the adjustment distances from the edges are much smaller than the screenhouse dimensions. Beyond this equilibration phase, the pertinent mean gradients to be resolved by any transport model are aligned with the vertical direction. There is now some indirect evidence that this assumption is valid inside large screenhouses ($\approx$400 m length scale) given the energy balance closure results reported by studies that employ the eddy-covariance method (Tanny et al. 2006). These idealized assumptions about the spatial extent of the screenhouse are invoked here so that general conclusions not 'pinned' to a particular configuration or screenhouse geometry can be derived from the model runs here.

The presence of a screen-roof, positioned at some distance above the canopy and parallel to the ground surface, modifies these vertical gradients, and this effect is the subject of the present investigation. To avoid the need for specifying a mixing length scale, which is complicated by the presence of a screen, and due to the possibility of 'counter-gradient' flows (Raupach 1989; Finnigan 2000; Siqueira et al. 2000), a second-order closure model is employed for all the flow variables. Moreover, unlike previous studies, the inclusion of a CO_2 budget is needed here to model the coupled photosynthesis and stomatal conductance at the leaf scale. The second-order closure formulation, the radiative and energy budgets, and the leaf-level equations are presented below.

2.1 Momentum Transport Model

For an extensive and uniform 'open' canopy in the absence of any screen, the one-dimensional, time- and horizontally-averaged conservation equation for the streamwise (x) momentum in the canopy is given by (Thom 1971):

$$\frac{\partial \overline{u}}{\partial t} = -\frac{\partial \overline{u'w'}}{\partial z} - F_{\mathrm{d,c}}, \tag{1}$$

where u and w are the streamwise and vertical components of the velocity respectively, the overbar denotes the time and horizontal averaging operator and primed quantities represent excursions from this average (Raupach and Shaw 1982). The $F_{\mathrm{d,c}}$ term denotes the drag force on the flow by the leaves given by:

$$F_{\mathrm{d,c}} = C_{\mathrm{d}} a \overline{u} \left|\overline{u}\right|, \tag{2}$$

where $a(z)$ is the leaf area density and C_{d} is the dimensionless drag coefficient for the leaves.

The canopy turbulence model used here is based on second-order closure principles for canopy flows in which the TKE is decomposed into two band frequencies, "turbulent shear kinetic energy" (SKE, low frequency) and "wake kinetic energy" (WKE, high frequency energy) as discussed in Wilson (1988) and Katul and Chang (1999). The WKE promoted by the canopy was included to account for the bypass (or short-circuit) of the usual turbulence energy cascade due to the intervention of drag elements (Poggi et al. 2004a, b, 2008; Poggi and Katul 2006; Cava and Katul 2008). The conversion of SKE (SKE is denoted here as k) to WKE is modelled as an additional dissipation term in the normal component of the stress equations (see below). No transport equation for WKE is needed because its feedback to SKE is assumed to be minimal (Wilson 1988). The budget equation for the tangential stress component and low-frequency band (SKE band) normal stress components is given by:

$$\frac{\partial \overline{u_i' u_j'}}{\partial t} = P_{ij} + R_{ij} + T_{ij} - \varepsilon_{ij}, \tag{3}$$

where the subscript refers to orthogonal coordinates, P is the production term, R is the redistribution term, T is the turbulent transport term, and ε is the dissipation term. The components of P, R and T used here are described in Wilson (1988), and, for completeness, their forms are given in Appendix A.

For the dissipation rate, ε_{ij}, special attention is required due to the presence of the screen. In the absence of the screen, the dissipation rate is decomposed into two contributions (Wilson 1988) given by:

$$\varepsilon_{ij} = \frac{2}{3}\varepsilon \delta_{ij} + \varepsilon_{c,ij}. \tag{4}$$

Here, ε is the viscous dissipation rate and the term $\varepsilon_{c,ij}$ represents the additional SKE to WKE transformation due to leaves, given by:

$$\varepsilon_{ij} = \frac{2}{3}\varepsilon \delta_{ij} + \left(2C_{\mathrm{d}} a \overline{u} \overline{u_i' u_j'} \delta_{ij} + 2C_{\mathrm{d}} a \overline{u} \overline{u_i' u_j'} \delta_{i1} \delta_{j1}\right), \tag{5}$$

with no summation implied over repeated indices. Contrary to previous closure models (Wilson 1988; Katul and Chang 1999), an actual transport equation for ε was used because the conventional surface-layer ε parametrization (Wilson 1988) may not hold for screen-house plantations due to the effects of the screen on the flow field. This equation is given by (Hanjalic and Launder 1972; Katul et al. 2004):

$$\frac{\partial \varepsilon}{\partial t} = \frac{\partial}{\partial z}\left(c_{\varepsilon 3}\frac{k}{\varepsilon}\overline{w'^2}\frac{\partial \varepsilon}{\partial z}\right) + c_{\varepsilon 1}\frac{\varepsilon}{k}\frac{P_{ii}}{2} - c_{\varepsilon 2}\frac{\varepsilon^2}{k}, \tag{6}$$

where $c_{\varepsilon 1}$, $c_{\varepsilon 2}$ and $c_{\varepsilon 3}$ are model constants that can be determined using arguments presented in Katul et al. (2004) and Sanz (2003).

The effects of the screen on the flow are modelled as a drag element intervention, similar to leaves. However, isotropy cannot be assumed because of the variations in screen geometry with respect to the airflow. Since the screen has different projected areas along different flow directions, the product between the screen drag coefficient, $C_{\mathrm{d,sc}}$, and the screen projected area, a_{sc}, is specified as a tensor with different values for each direction. The additional terms to Eqs. 1 and 4 needed to account for the screen effects are, respectively, given by:

$$F_{\mathrm{d,sc}} = \left(C_{\mathrm{d,sc}}a_{\mathrm{sc}}\right)\overline{u}\,|\overline{u}|\,, \tag{7}$$

$$\varepsilon_{\mathrm{sc},ij} = \left[2\left(C_{\mathrm{d,sc}}a_{\mathrm{sc}}\right)_i\overline{u}\overline{u'_i u'_j}\delta_{ij} + 2\left(C_{\mathrm{d,sc}}\,a_{\mathrm{sc}}\right)_i\overline{u}\overline{u'_i u'_j}\delta_{i1}\delta_{j1}\right]. \tag{8}$$

Equation 3, along with Eqs. 1, 6, 9 and 13 (the latter two described later), are solved numerically for the three velocity-component variances (normal stresses), $\overline{u'^2}$, $\overline{v'^2}$, $\overline{w'^2}$ and the streamwise-vertical velocity-component covariance (tangencial stress), $\overline{u'w'}$, using a finite-volume discretization technique. The screen is assumed to have its area distributed over a single finite-volume numerical cell.

2.2 Scalar Transport Model

The one-dimensional, time- and horizontally-averaged conservation equation for a scalar quantity in a canopy flow is given by (Meyers and Paw 1987; Baldocchi and Meyers 1998):

$$\frac{\partial \overline{c}}{\partial t} = -\frac{\partial \overline{w'c'}}{\partial z} + S_c + S_{\mathrm{sc}}, \tag{9}$$

where c is a generic scalar being the air temperature (surrogate for internal energy), water-vapour mixing ratio or CO_2 concentration, S_c is a local source/sink of scalar c within the canopy volume and S_{sc} is source/sink due to the screen, applicable only for sensible heat, distributed exclusively over a single finite-volume numerical cell corresponding to the screen location. In fact, the screen could serve as a source or sink for water vapour as well if precipitation interception, dew and evaporation of water retained on the screen surface are considered. Since the case study here is a screenhouse used for water savings in a semi-arid region it is unlikely that any of these processes occur. The source terms are given by:

$$S_c = 2aG\left(c_{\mathrm{L}} - \overline{c}\right), \tag{10}$$

$$S_{\mathrm{sc}} = 2\phi g_{\mathrm{sc}}\left(T_{\mathrm{sc}} - \overline{T}\right), \tag{11}$$

where c_{L} is the leaf scalar concentration, G is the leaf conductance, T_{sc} is the screen temperature, ϕ is the screen solidity and g_{sc} is the screen boundary-layer conductance (analogous to the convective heat transfer coefficient), given in s^{-1} because it incorporates screen thickness distributed over the finite-volume numerical cell. The G is estimated with a resistance (inverse of G) model comprised of a leaf boundary-layer resistance and a stomatal resistance arranged in series.

The leaf boundary-layer conductance is estimated using flat-plate theory for a laminar boundary layer given by (Campbell and Norman 1998):

$$g_{\mathrm{bl}} = \frac{0.664 \rho \chi_N N^{1/3} Re^{1/2}}{l_{\mathrm{bl}}}, \tag{12}$$

where χ_c is the molecular diffusivity of the scalar (heat, water vapour or CO_2) in air, ρ is the mean air density, Re ($= \overline{u} l_{\mathrm{bl}}/\nu$) is a local leaf Reynolds number assumed to be smaller than the critical Reynolds number for the transition from laminar to turbulent flow regime and l_{bl} is a characteristic leaf dimension (see Table 1 for values). The parameter N is either the molecular Prandtl number for sensible heat or Schmidt number for other scalars. Stomatal resistance is determined from a physiological model described later.

For the scalar turbulent flux, the budget equations are expressed as (Meyers and Paw 1987):

$$\frac{\partial \overline{w'c'}}{\partial t} = -\overline{w'^2}\frac{\partial \overline{c}}{\partial z} - \frac{\partial}{\partial z}\left(c_{\mathrm{s}}\frac{k}{\varepsilon}\left(\overline{w'^2}\frac{\partial \overline{w'c'}}{\partial z}\right)\right) - c_{\theta 3}\frac{\varepsilon}{k}\overline{w'c'}, \tag{13}$$

where c_{s} and $c_{\theta 3}$ are model constants. This budget equation follows a structure similar to Eq. 3, namely it comprises of production, transport and dissipation terms, except that, in the case of scalars, there is no pressure redistribution term.

To model the microclimate inside the screenhouse, air temperature, water-vapour mixing ratio and CO_2 concentration transport equations must be simultaneously solved as scalars. In the case of air temperature (water vapour and CO_2 are discussed later, see Sect. 2.3), only the boundary-layer resistance is considered in the estimation of G because the source of internal energy to canopy air is the heat exchange between the leaf surface and canopy air

Table 1 Physical and physiological properties of the banana plantation used in the simulations

Parameter	Symbol (unit)	Value
Canopy height	H (m)	4[a]
Leaf area index	LAI	3[a]
Characteristic leaf dimension	l_{bl}(m)	0.5[b]
Leaf absorptivity to PAR	α_{p}	0.8[c]
Maximum quantum efficiency	e_{m}	0.08[c]
Maximum catalytic capacity of Rubisco at 25°C	$V_{\mathrm{cmax},25}$(μmol m^{-2}s^{-1})	1249[d]
Ratio of respiration and catalytic capacity	β	0.003[d]
Temperature dependence of V_{cmax} parameter	a_1	0.088[e]
Temperature dependence of V_{cmax} parameter	a_2	0.29[e]
Residual stomatal conductance	b (mol m^{-2}s^{-1})	0.01[f]
Sensitivity of conductance to humidity deficit	D_0 (kPa)	3.0[f]
Leuning conductance model parameter m	m	1[g]

[a] From Tanny et al. (2010)
[b] Visual inspection
[c] From Campbell and Norman (1998)
[d] From Turner et al. (2007)
[e] From Lai et al. (2002)
[f] From Leuning et al. (1995), a value that reflects high leaf-nitrogen content
[g] Reduced from Leuning (1995) to account for to vegetation acclimation

Table 2 Radiative and drag properties of the screen

Parameter	Symbol	Value
Solidity	ϕ	0.3
Transmissivity to diffuse shortwave[a]	$\tau_{\mathrm{SW,d}}$	0.45
Reflectivity to shortwave	$\rho_{\mathrm{sc,SW}}$	0.2
Transmissivity to longwave	$\tau_{\mathrm{LW,d}}$	0.45
Reflectivity to longwave	$\rho_{\mathrm{sc,LW}}$	0.05
Emissivity	e	0.45
Drag in longitudinal direction[b,c]	$(C_{\mathrm{d,sc}}a_{\mathrm{sc}})_x$	0.02
Drag in transversal direction[b,d]	$(C_{\mathrm{d,sc}}a_{\mathrm{sc}})_y$	0.02
Drag in vertical direction[b,c,d]	$(C_{\mathrm{d,sc}}a_{\mathrm{sc}})_z$	0.08

Radiative properties were derived from a short experiment, in which shortwave and longwave radiative fluxes were measured above and below the screen (see Apenedix B and Fig. 2)
[a] Note that the transmissivity to beam shortwave is a function of zenith angle ψ (see Fig. 3)
[b] $C_{\mathrm{d,sc}}a_{\mathrm{sc}}$ parameter has units of $[\mathrm{m}^{-1}]$
[c] These values were estimated to provide reasonable velocity statistics
[d] The value of the vertical direction was assumed higher due to the fact that the screen projected area is greater in the vertical direction for the finite volume in which screen is located

around it. Additionally, since the screen is considered as a drag element (see Table 2 for drag parameters), it becomes a heat source requiring the calculation of its own boundary-layer resistance. This boundary-layer resistance varies with the mean velocity at the screen height and is estimated assuming a flat plate analogy but with forced convection (*Re* greater than a critical Reynolds number) with the formulation given in Incropera and Witt (1996).

Furthermore, soil surface temperature, soil evaporation, and CO_2 respiration are required as boundary conditions for the air temperature, water vapour, and CO_2 mean scalar budget equations. The skin temperature of the soil-plant system is also needed for the radiation exchange. A one-dimensional soil heat equation that combines Fourier's heat conduction law with a soil heat budget (Siqueira et al. 2006) is incorporated into the model to compute the soil temperature profile. Soil respiration is assumed to exponentially vary with soil temperature. Soil evaporation is neglected (Tanny et al. 2006) given the fact that soil is generally moist only near the drip line zone, which is mostly shaded by the plants. However, it can be readily added if the soil evaporation is energy limited.

2.3 Physiological Model

To estimate c_{L} (scalar values at the leaf surface, see Eq. 10), it is necessary to include a leaf energy balance for finite volumes within the canopy, and a photosynthesis model. The former is given as:

$$m_{\mathrm{L}} C_{\mathrm{leaf}} \frac{\mathrm{d}T_{\mathrm{L}}}{\mathrm{d}t} = R_{\mathrm{N}} - S_{\mathrm{T}} - L_{\mathrm{v}} S_{\mathrm{M}}, \tag{14}$$

where m_{L} is the leaf mass present in the finite volume, C_{leaf} is the specific heat of the leaf (assumed similar to water), R_{N} is net radiation absorbed by the leaves (obtained from a radiation transfer model, see Sect. 2.4 below), S_{T} and S_{M} are the sensible heat and water vapour lost to the air in the vicinity of the leaves and L_{v} is the latent heat of vaporization of water. Leaf-intercellular space is considered saturated, so the water-vapour mixing ratio in

leaf-intercellular spaces is the mixing ratio corresponding to the saturation pressure at leaf temperature T_L.

A photosynthesis model is also required to compute the leaf-level sources/sinks of CO_2 and water vapour and these models are now widely used with turbulence closure schemes (Juang et al. 2008). The leaf-level net photosynthesis (A_n) is given by the biochemical demand function (Farquhar et al. 1980):

$$A_n = \frac{\kappa_1 (C_L - \Gamma^*)}{C_L - \kappa_2} - R_d, \tag{15}$$

where R_d is the dark respiration rate, Γ^* is the CO_2 compensation point in the absence of mitochondrial respiration (i.e. CO_2 concentration at which net photosynthesis is zero) and is given by $\Gamma^* = C_{oa}/(2\tau_t)$ with $\tau_t = 2.6 \exp(-0.056 (T_L - 298))$, T_L in K, C_{oa} is the oxygen concentration in air, and C_L is the leaf intercellular CO_2 concentration. The parameters $\kappa_1 = \alpha_p e_m I_p$ and $\kappa_2 = 2\Gamma^*$ for light-limited photosynthesis; $\kappa_1 = V_{cmax}$ and $\kappa_2 = K_C (1 + C_{oa}/K_O)$ when the assimilation rate is limited by Rubisco activity, where α_p is the leaf absorptivity for photosynthetically active radiation (PAR), e_m is the maximum quantum efficiency, I_p is the incident PAR flux density on the leaf surface (fraction of short-wave radiation at the visible spectral band converted to flux density), V_{cmax} is the maximum catalytic capacity of Rubisco per unit leaf area, and K_C and K_O are Michaelis–Menten constants for CO_2 fixation and for oxygen inhibition with respect to CO_2. R_d can be estimated from V_{cmax} using (Farquhar et al. 1980):

$$R_d = \beta\, V_{cmax}, \tag{16}$$

where β is a constant. The value of V_{cmax} is temperature dependent and is approximated by (Campbell and Norman 1998):

$$V_{cmax} = V_{cmax,25} \frac{\exp[a_1 (T_L - 298)]}{1 + \exp[a_2 (T_L - 314)]}, \tag{17}$$

where $V_{cmax,25}$ is the V_{cmax} at 25°C and the a_1 and a_2 are model constants (Campbell and Norman 1998).

The stomatal conductance needed for the calculation of water vapour and CO_2 sources/sinks is given by (Leuning 1995):

$$g_{s,c} = m \frac{A_n}{(C_s - \Gamma^*)\left(1 + \frac{D_s}{D_0}\right)} + b, \tag{18}$$

where D_s and C_s are vapour pressure deficit and CO_2 concentration at the leaf surface respectively, m is a physiological constant that varies across species, b is a residual stomatal conductance, and D_0 is an empirical coefficient related to the sensitivity of the stomatal conductance to D_s. This model applies for well-watered crop conditions as discussed in Juang et al. (2008), which is often the case in screenhouses. Other leaf-level stomatal conductance models that relate $g_{s,c}$ to A_n/C_s can replace Eq. 18 when deemed more suitable. These $g_{s,c} - A_n/C_s$ relationships are presented elsewhere and are not elaborated upon here (Katul et al. 2009, 2010). Table 1 provides the values of the bio-physiological parameters used in the model calculations. The up-scaling from leaf-level rates to S_c is conducted using $a(z)$ as a scaling parameter.

2.4 Radiative Transfer Model

A multi-layered-canopy shortwave radiation attenuation model was used to represent the shortwave exchange between the vegetation and the atmosphere (Leuning et al. 1995; Wang and Leuning 1998). The model decomposes the incoming solar shortwave (SW_{sun}) into direct beam and diffuse radiation due to the fact that canopy attenuation is different for each of these components. For the longwave thermal radiation exchange within the canopy, a similar attenuation model is also implemented (Campbell and Norman 1998), but longwave is computed independently for the upward and downward fluxes and includes the emission from the canopy elements.

The screen modulation on incoming radiation is described by:

$$SW_{\mathrm{b}} = SW_{\mathrm{sun,b}}\,(1-\phi), \tag{19}$$

$$SW_{\mathrm{d}} = SW_{\mathrm{sun,d}}\,(1-\phi) + \left[SW_{\mathrm{sun,b}}\tau_{\mathrm{SW,b}} + SW_{\mathrm{sun,d}}\tau_{\mathrm{SW,d}}\right]\phi, \tag{20}$$

$$LW = LW_{\mathrm{sky}}\,(1-\phi) + LW_{\mathrm{sky}}\phi\;\tau_{\mathrm{LW}} + \phi e\sigma_{\mathrm{SB}}T_{\mathrm{sc}}^4, \tag{21}$$

where SW_{b}, SW_{d}, LW are direct beam solar radiation, diffuse solar radiation and longwave radiation respectively reaching canopy top, the subscripts sun and sky refer to incoming solar and atmospheric radiation (reaching the screen) respectively, σ_{SB} is the Stefan–Boltzmann constant, $\rho_{\mathrm{sc,SW}}$ is the screen-material reflectivity to shortwave, e is the screen-material emissivity and τ_{SW} and τ_{LW} are the screen-material transmissivity to shortwave and longwave radiation respectively. Because the canopy responds differently to direct beam and diffuse shortwave radiation and τ_{SW} may vary as a function of the zenith angle, τ_{SW} to direct beam ($\tau_{\mathrm{SW,b}}$) and to diffuse ($\tau_{\mathrm{SW,d}}$) shortwave radiation are used independently to calculate SW_{b} and SW_{d}, respectively.

2.5 Screen Energy Balance

Since screen temperature is required to compute the heat source to the air within the finite-volume computational cell at which the screen is located and also to estimate screen longwave emission, an energy budget for the screen is required and is given by:

$$\begin{aligned} c_{\mathrm{sc}}\frac{\mathrm{d}T_{\mathrm{sc}}}{\mathrm{d}t} = {} & \left[SW_{\mathrm{sun,b}}\left(1-\rho_{\mathrm{sc,SW}}-\tau_{\mathrm{SW,b}}\right) + SW_{\mathrm{sun,d}}\left(1-\rho_{\mathrm{sc,SW}}-\tau_{\mathrm{SW,d}}\right)\right]\phi \\ & + \left(LW_{\mathrm{sky}} + LW_{\mathrm{can}}\right)\left(1-\rho_{\mathrm{sc,LW}}-\tau_{\mathrm{LW}}\right)\phi - 2\phi e\sigma_{\mathrm{SB}}T_{\mathrm{sc}}^4 - S_{\mathrm{sc}}, \end{aligned} \tag{22}$$

where c_{sc} is the specific heat of the screen material, LW_{can} is the longwave radiation outgoing from the canopy volume and S_{sc} is the turbulent heat flux from the screen accounted as a heat source to the air.

2.6 Case Study and Model Runs

As a case study, the system of differential equations is numerically solved for two banana plantations: one considered 'open' and another is 'screened'. The choice of a banana screenhouse as a case study is due to the fact that it is becoming a common practice in irrigated cultivation within arid and semi-arid regions such as the Mediterranean area. The attributes of the banana plantation used in the model calculations here resemble those reported for a large screenhouse in northern Israel (Tanny et al. 2006, 2010). At maximum leaf area index ($\approx$3.0 $\mathrm{m^2\ m^{-2}}$), the mean crop height was about 4 m and the screen height was about 2 m above the mean crop height. With such a tall canopy relative to the height of the screen,

Table 3 Daily assimilation (*GPP*), plant transpiration (*TR*) and water-use efficiency (*WUE*) for the four modelled test cases

Setup	*GPP*(gC $m^{-2}d^{-1}$)	*TR* (g $m^{-2}d^{-1}$)	*WUE*
Open	1.52×10^{-4}	1.47×10^{3}	1.03×10^{-7}
Screened	1.29×10^{-4}	1.00×10^{3}	1.29×10^{-7}
Radiation only	1.44×10^{-4}	1.39×10^{3}	1.04×10^{-7}
Momentum only	1.35×10^{-4}	1.05×10^{3}	1.29×10^{-7}

Table 4 Turbulence-model empirical parameters

Parameter	C_d	c_1	c_2	c_1'	$c_{\varepsilon 1}$	$c_{\varepsilon 2}$	$c_{\varepsilon 3}$	c_s	$c_{\theta 3}$
Value	0.1[a]	1.8[b]	0.6[b]	0.5[b]	1.44[c]	1.92[c]	0.16[d]	0.11[b]	9.9[e]

[a] Tuned
[b] From Wilson (1988)
[c] From Katul et al. (2004)
[d] From Gibson and Rodi (1981)
[e] From Meyers and Paw (1987)

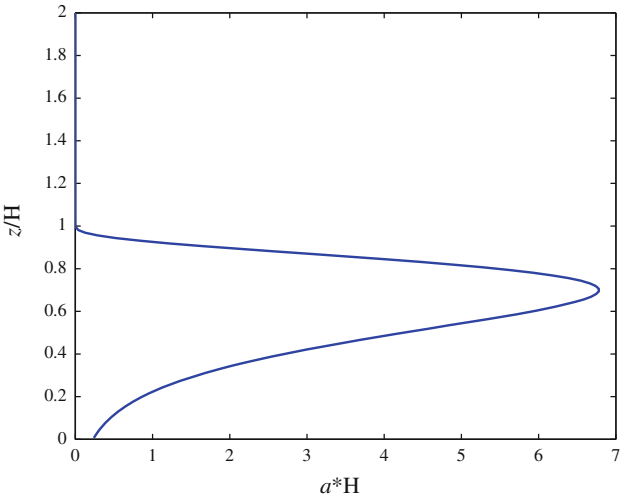

Fig. 1 Normalized leaf area density (a) profile for the banana plantation used in the simulations, where H is the canopy height

the momentum and scalar internal boundary layers adjust over short distances (Hsieh and Katul 2009; Manzoni et al. 2011). The relevant closure constants, radiative properties, and the physical and physiological properties of the screen and the banana plantation derived or used in the model runs are summarized in Tables 1, 2, 3, and 4. The other parameters are standard values taken from the literature. The normalized leaf area density profile used in the simulation, shown in Fig. 1, was determined as a gamma distribution function with shape parameter set to 4 and scale parameter set to 1. These parameter values were chosen to reflect the fact that, from visual inspection of banana plantations, there is maximum foliage in the upper part of the canopy and very little foliage close to the ground.

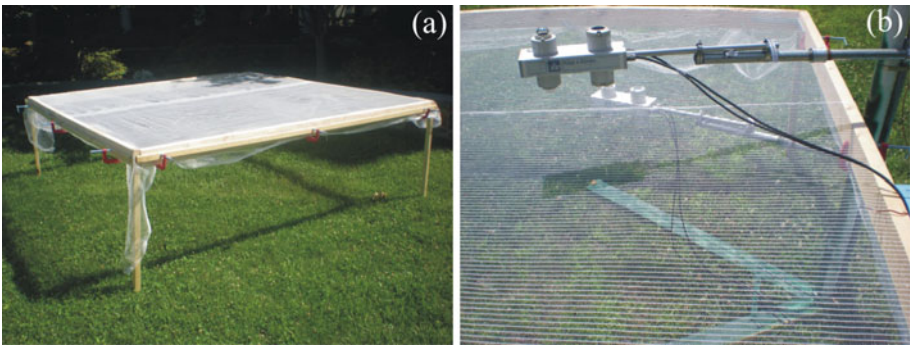

Fig. 2 The experimental set-up for the determination of the screen radiative properties. The screen was framed (**a**) and two CNR1 radiometers measuring all the components of the radiative balance were positioned above and below the screen (**b**)

The screen properties required to solve Eqs. 19 to 22 are selected for a screen model *Combined Clear Net 13% 3.2 M* currently in use for banana screenhouses (manufactured by Polysack, Israel). The screen solidity ϕ was determined from image processing of digital figures obtained by scanning a portion of the screen. To estimate the screen radiation properties, an intensive field experiment was performed in which a 5.94-m^2 screen was framed and positioned about 0.8 m above a grass surface (Fig. 2a) in a clearing at Duke University, Durham, North Carolina, USA. Radiation components (longwave and shortwave), both incoming and outgoing, were measured over and under the screen with two Kipp & Zonen CNR1 net radiometers (Fig. 2b). The net radiometers were matched by making measurements for two days with the set-up but with no screen. Additionally, two thermocouples were employed, one measuring air temperature and the other mingled with the screen; these were used to estimate screen temperature. Data were collected for two full days (June 23 and June 24, 2009) and the screen radiation properties were estimated using a procedure described in Cohen and Fuchs (1999). For completeness, the formulation to estimate the radiation properties is presented in Appendix B. Contrary to $\tau_{\mathrm{SW,d}}$, $\tau_{\mathrm{SW,b}}$ may vary with zenith angle, so $\tau_{\mathrm{SW,b}}$ was determined as a function of zenith angle (see Appendix B). The regression results for this relationship are shown in Fig. 3. The radiation properties, except for $\tau_{\mathrm{SW,b}}$ given in Fig. 3, are obtained from the data using the procedure described in Appendix B (see Table 2 for values). Also included in Table 2 is the product of the screen drag coefficient and screen projected surface area ($C_{\mathrm{d,sc}}a_{\mathrm{sc}}$) for the three spatial directions. With the lack of detailed experimental data to estimate $C_{\mathrm{d,sc}}$ (projected areas could be calculated from image processing), the values of the products were obtained from test runs to provide reasonable velocity statistics, such as those reported by Tanny et al. (2010) in a banana screenhouse that employed such a screen.

The flow field for the open and screened soil-plant systems was modelled a priori since all buoyancy effects were neglected (neutral stability) initially making the temperature and velocity statistics decoupled. The neutral-stability conditions may not prevail at all times since these conditions require strong mechanical turbulence generation when compared to thermal effects. However, for the purpose of our investigation, neutral stability is a reasonable approximation given the small heights above the plant surface within the screenhouse. Furthermore, neutral stability is likely to be the case for the periods where most of the exchange processes occur, provided strong winds prevail during daytime.

For the purpose of comparisons between the open and screened model runs, the flow speed at the upper boundary set at five times the canopy height was the same for the open and

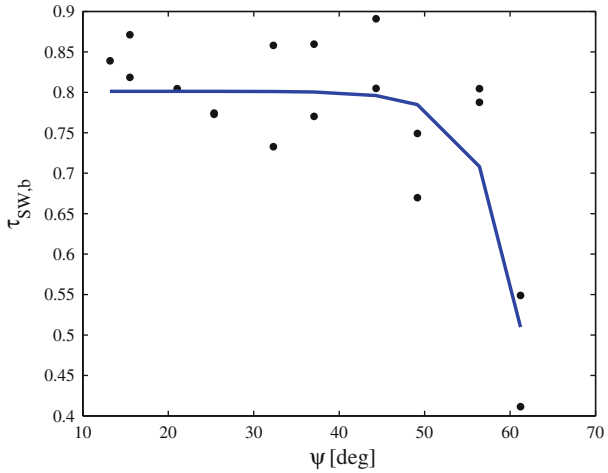

Fig. 3 The measured screen transmissivity to direct incoming solar shortwave radiation ($\tau_{SW,b}$) as a function of zenith angle (ψ)

screened systems. The reason for this choice versus a friction velocity boundary condition is that differences in surface roughness caused by the presence of a screen can affect momentum transfer and, consequently, the friction velocity.

3 Results and Discussion

For the case studied here, model runs are used to explore how the presence of a screen alters the mean flow field, turbulent stresses, radiative and energy fluxes, as well as scalar sources, sinks, fluxes, and mean concentration. Whether these screen-induced modifications are primarily related to the radiation-energy balance versus the aerodynamic effects is discussed below.

3.1 The Mean and Turbulent Flow Field

The mean velocity profile shown in Fig. 4 shows reduced speeds in the air space between the screen and the top of the canopy, in comparison with its open canopy counterpart. However, the mean velocity profile re-adjusts over a short vertical distance above the screen to its open canopy state. This is not entirely surprising given that the overall effect of the screen translates into an elevated but smoother surface when compared to the exposed canopy (Tanny and Cohen 2003; Tanny et al. 2009). In fact, the modelled friction velocity for the screened case needed to maintain the same mean velocity at the top boundary (well above the screen) is about 70% of that for the open plantation. This is in general agreement with the 60% ratio obtained by Tanny and Cohen (2003) for a small shade net covering a citrus orchard under neutral stability (see their Fig. 6). The velocity-component standard deviations and turbulent shear-stress profiles are presented in Fig. 5, and show similar attenuation inside the canopy but diverge in the air space between the canopy top and the screen. Above the screen height, the profiles of velocity statistics tend to recover similar roughness sublayer behaviour as in the absence of a screen. It should be emphasized that these figures are normalized by the

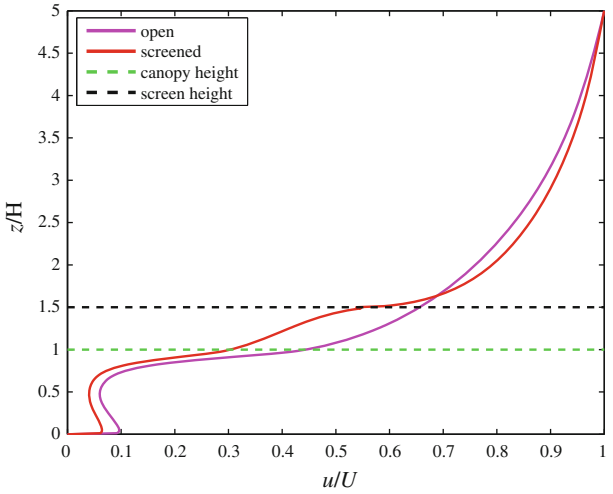

Fig. 4 The modeled streamwise mean velocity profile normalized by the velocity at the upper boundary condition set at $5H$, where H is the canopy height

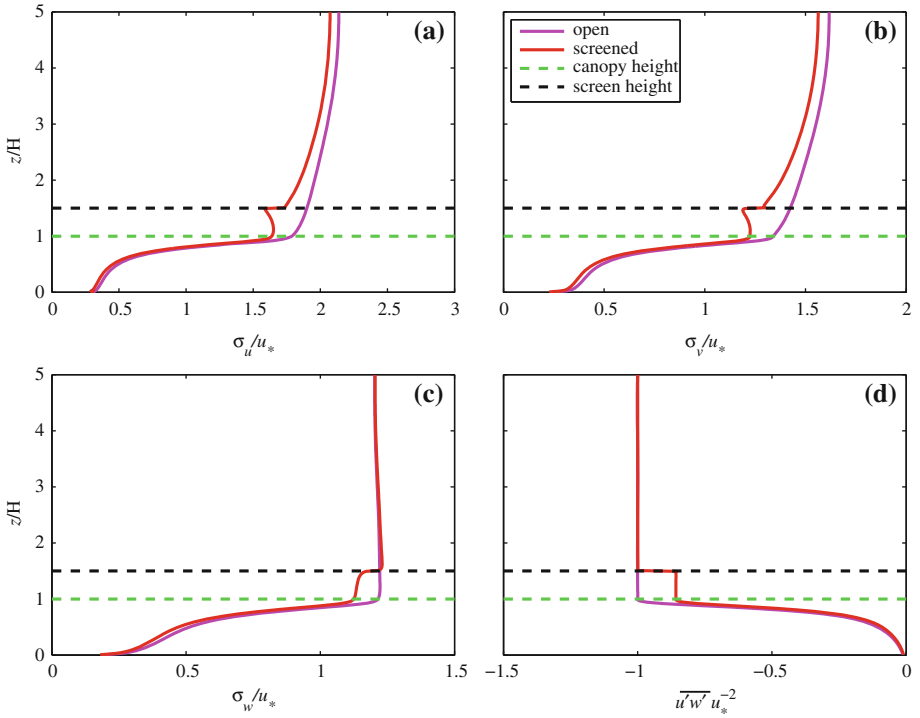

Fig. 5 Profiles of the normalized Reynolds stress tensor components, where the velocity standard deviation (e.g. $\sigma_u = \sqrt{u'^2}$) and the turbulent shear-stress profiles are normalized by friction velocity u_* defined at the canopy top

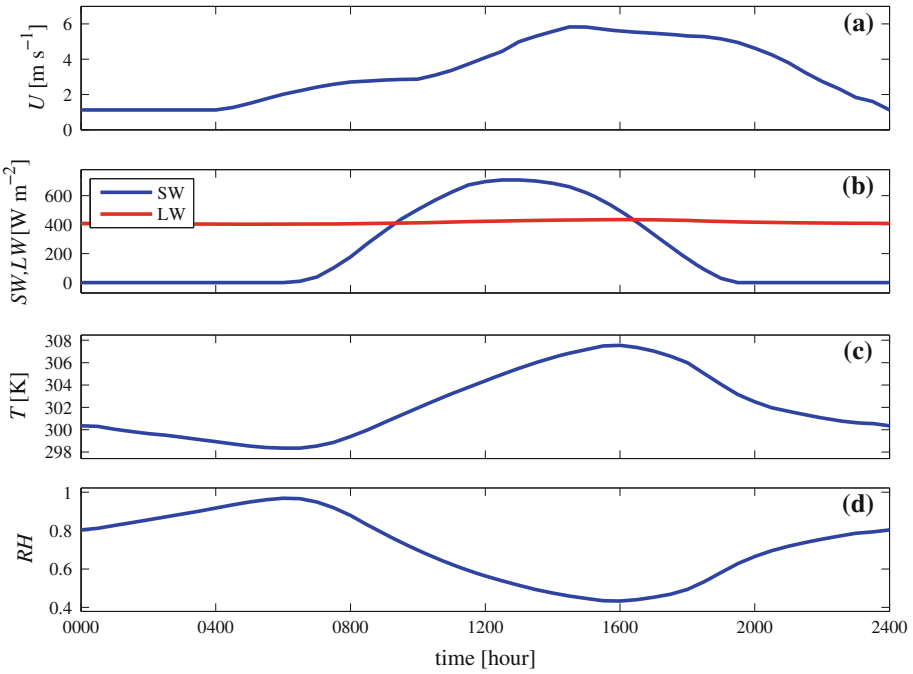

Fig. 6 The periodic meteorological forcing time series used in the model runs. These variables represent the upper boundary conditions (BC) at 20 m (or $5H$) above the ground. Here, U is streamwise velocity (**a**), SW and LW are the incident shortwave and longwave radiation, respectively (**b**), T is the mean air temperature (**c**), and RH is the mean air relative humidity (**d**)

friction velocity at the canopy top, which is not identical for the screened and open systems as earlier noted.

3.2 Scalars and Their Exchange Rates

The model runs were performed for a 10-day time span with repeated daily meteorological forcing specified at the upper boundary as given in Fig. 6. The daily variations of the meteorological forcing were estimated from ensemble averaging of measurements in the experiment reported by Tanny et al. (2010). Longwave fluxes from the sky were estimated from air temperature and relative humidity assuming an atmospheric emissivity formulation. The results discussed here represent the last day of the simulations. The first nine days were needed for a 'spin-up' time to ensure that the daily cycle has attained a stationary state, especially important for soil temperature. Soil was assumed to have 0.7-m depth, and soil respiration was estimated from the average soil temperature because it was considered that the root respiration would be the major source of soil respiration. Soil longwave emission was computed from the soil surface temperature.

The effect of the screen on the internal mean air temperature is evident in Fig. 7, which shows the contour plots of mean air temperature as a function of time and height. The screen promotes increases in mean air temperature during the day inside the screenhouse as expected, and this is a consequence of a combination of factors. On the one hand, there is the modulation of the screen on the radiative transfer, which has two concurrent effects, namely, the reduction of incoming radiation (both shortwave and longwave) by shading, and the

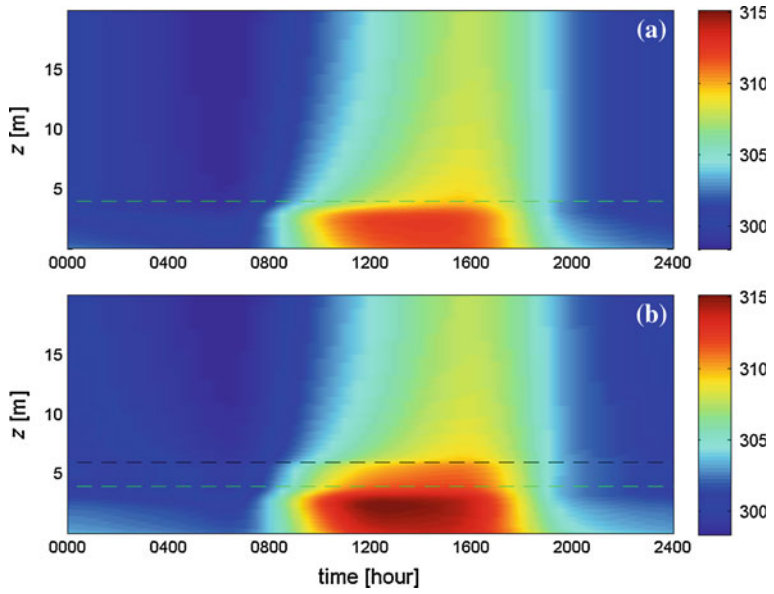

Fig. 7 Diurnal variation of the mean air temperature (in K) profile for the open- (**a**) and screened- (**b**) system runs. *Dashed lines* represent the canopy top (*green*) and screen (*black*) heights

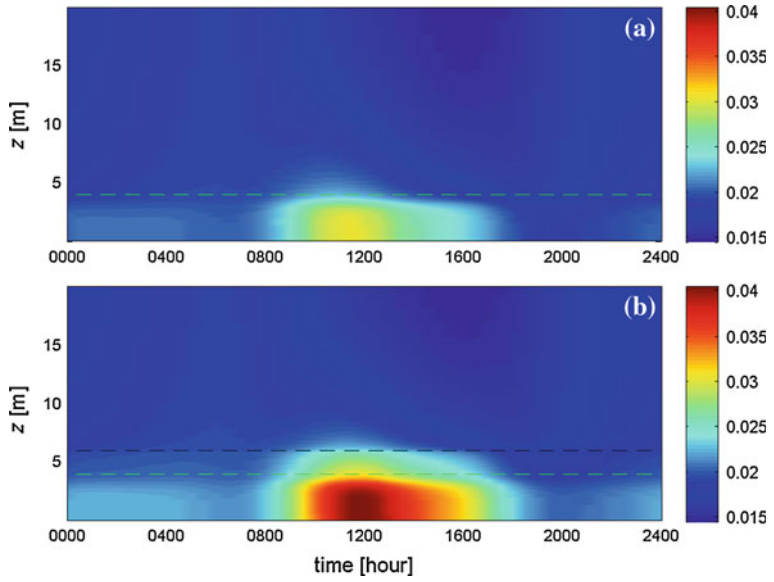

Fig. 8 Similar to Fig. 7 but for water-vapour mixing ratio (in kg kg^{-1}) distribution

retention of the longwave emitted by the surface (soil and canopy). Additionally, the turbulent diffusivity is reduced due to the screen drag acting on the flow field, which has a marked influence on the velocity statistics as demonstrated above. The latter effect is also evident in the other two scalars, mean water vapour mixing ratio and the mean CO_2 concentration, whose distributions are presented in Figs. 8 and 9, respectively. The water vapour transpired

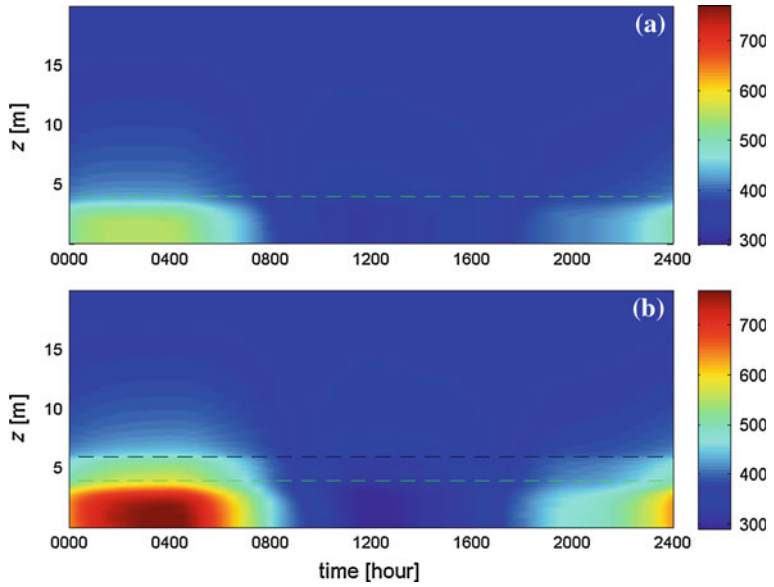

Fig. 9 Similar to Fig. 7 but for CO_2 concentration (in ppm) distribution

by the vegetation is 'retained' inside the screenhouse due to the reduced turbulent transport. Since transpiration is a diffusion process, the higher water-vapour mixing ratio maintained inside the screenhouse leads to irrigation water savings, as is shown later.

A similar effect is also evident for the mean CO_2 concentration inside the screenhouse. However, because the soil-plant system can act as a source and a sink during the course of the day, the resulting CO_2 concentration is not identical to its water-vapour counterpart. During the evening hours, the CO_2 soil efflux and the above-ground respiration promote a large CO_2 accumulation within the screenhouse, at least when compared with the open system. However, during daytime conditions, photosynthesis consumes this excess CO_2 and, because CO_2 transport from above is reduced by the presence of the screen, the CO_2 is actually more depleted within the screenhouse. In essence, the reduced turbulence mixing within the screenhouse increases the residence time of CO_2 molecules, including those originating from soil and plant nocturnal respiration, thereby permitting leaf photosynthesis to act on them.

In terms of the overall energy exchange, the consequences of the presence of a screen are demonstrated in Fig. 10a–c. The modelled diurnal courses in net radiation (Fig. 10a), sensible heat flux (Fig. 10b) and latent heat flux (Fig. 10c) above the canopy are presented for the open and screened systems. The modelled net radiation and sensible heat flux time series below the screen are also shown to emphasize the role of the screen energy and radiation balances. The differences between the unscreened and screened sensible heat flux time series are primarily due to the turbulent heat exchange between the screen and the air in the screen's vicinity. Since the energy balance is enforced in the present formulation, and because the daily cycle is in stationary state, after the 9-day spin-up period, the summation of latent and sensible heat fluxes integrated over the day must match the daily-integrated net radiation. Clearly, there is a strong reduction of both sensible heat and latent heat fluxes when a screen is employed.

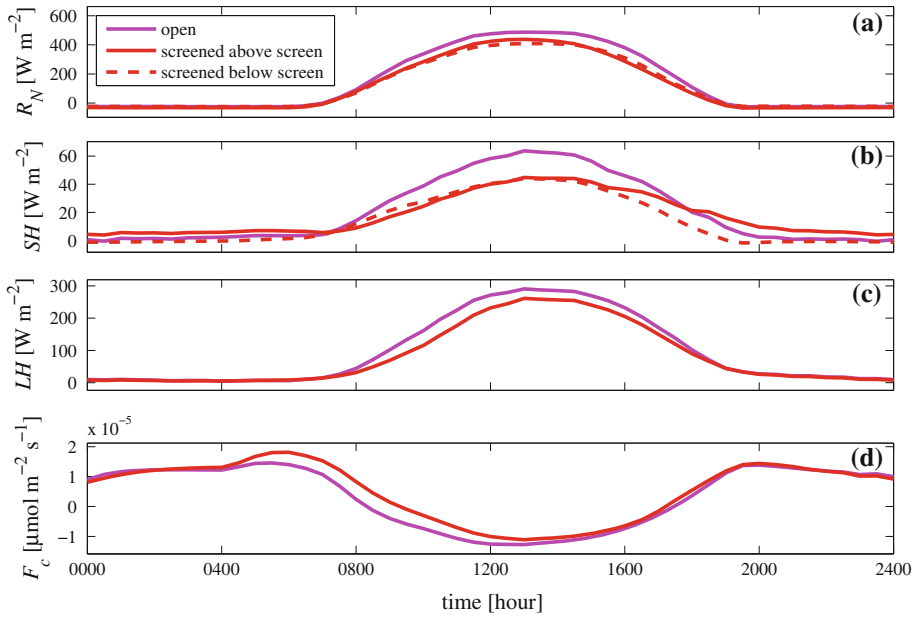

Fig. 10 Net radiation (R_N, **a**), sensible heat (SH, **b**), latent heat (LH, **c**) and CO_2 (F_c, **d**) fluxes at the upper boundary for the two cases, open and screened plantations. The sensible heat flux in the space between the canopy and the screen is also shown for the screened plantation

As far as carbon dioxide exchange is concerned, the presence of the screen has interesting consequences not previously noted or explored (Fig. 10d). Early in the morning, the carbon dioxide 'flushing' from the canopy is actually stronger for the screened plantation due to the higher nocturnal CO_2 accumulation. During the morning, the CO_2 fluxes towards the canopy are actually reduced compared to the open plantation because of the effects of the screen on the turbulent transport. Later in the afternoon, CO_2 fluxes actually 'catch-up' in the screen house with their open field counterpart because of higher CO_2 depletion (and hence gradient) inside the screenhouse.

3.3 Screen Effects: Radiative or Aerodynamic?

To address the questions that framed the scope here, two additional model runs were performed. One considered only the radiation effects of the screen and neglected the screen drag (assuming $C_{d,sc}a_{sc} = 0$) and another assumed a completely transparent screen but retained its anisotropic drag effects on the flow. To achieve a 'transparent screen', the radiative parameters were selected as follows: $\tau = 1$, $\rho_{sc} = 0$ (for both longwave and shortwave), and $e = 0$.

The flux comparisons are presented in Fig. 11. Based on these runs, the screen interference on the flow field appears to have a stronger effect than the screen radiation modulation on the sensible heat transfer, as evidenced in Fig. 11a. This might be a compensation of opposing screen radiation effects, reduction of incoming shortwave by shading, contributing to a reduction in R_N, and reduction of outgoing longwave due to the screen, contributing to an increase in R_N. It is associated with the specific screen considered and may change with screen radiative properties. Irrespective, this fact highlights the importance of the proper

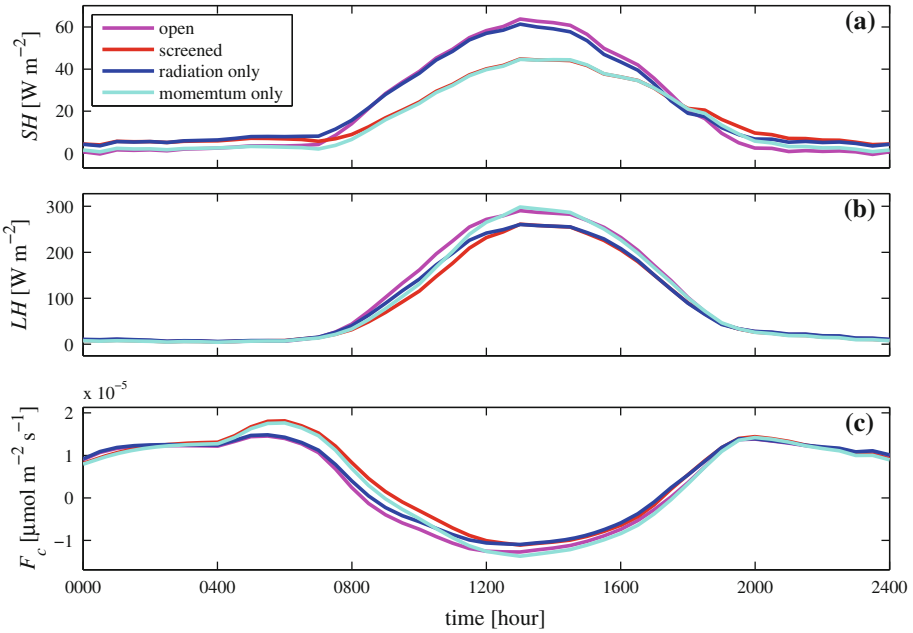

Fig. 11 Similar to Fig. 10 but including fluxes modeled with radiation modulation only (radiation only, *blue lines*) and with screen effects on flow field only (momentum only, *cyan lines*)

characterization of the screen aerodynamic properties and the need for characterizing the flow field in such problems.

For latent heat fluxes, radiation modulation only affected the water-vapour exchange indirectly through changes in the canopy microclimate. The consequences of these factors promoted interesting latent heat effects (Fig. 11b). During the morning hours, both radiation and wind speed had similar effects on the water-vapour transport, though in the afternoon, radiation modulation appears to have a stronger impact on water exchange.

In terms of CO_2 fluxes, a number of intriguing features are highlighted by these model runs (Fig. 11c). During early morning periods, most of the screen modulation is due to differences in turbulent transport properties. Later in the morning, after 1000 local time, both aerodynamic and radiative effects contribute equally. Late in the afternoon, around 1600 local time, interestingly, the two effects appear to compensate each other and the CO_2 exchange in the screenhouse plantation approximates to the open plantation. It is worth noting that all processes are coupled and non-linear, so "contributions" cannot be linearly combined.

The effectiveness of the screenhouse in terms of water savings can be assessed in a number of ways. Here, the so-called water-use efficiency (WUE), which is defined as the carbon uptake by the plant per unit water loss by transpiration, was chosen. Table 3 shows daily (last day) values of gross primary productivity (GPP), transpiration (TR), and WUE for the four model runs. The model results suggest that reductions in assimilation are strongly related to the reduced turbulent transport. However, because most of the water savings are also related to the changes in the velocity statistics, water-use efficiency gains in screenhouse plantations are directly related to effects of the screen on the turbulent transport characteristics. The 30% increase in WUE of the screened plantation as compared to the open plantation (Table 3) is in general agreement with recent field data obtained for banana plantations in northern Israel

(Y. Israeli, private communication, 2011). In these field experiments, WUE was estimated as the ratio between total yield and total irrigation accumulated during several seasons. The results showed that in the screenhouse, irrigation could be reduced by about 30% with almost no change in yield. It is worth noting that, although GPP does not exactly reflect yield, it is positively correlated with yield given the connection between yield (biomass at harvest) and photosynthesis (main term responsible for biomass accumulation).

In fact, an order of magnitude estimate of WUE is given as:

$$WUE = \frac{GPP}{TR} \approx \frac{C_{\mathrm{a,can}}}{D_{\mathrm{a,can}}}\left(1 - \frac{C_{\mathrm{L,can}}}{C_{\mathrm{a,can}}}\right), \tag{23}$$

where $C_{\mathrm{a,can}}$ is the mean canopy-air CO_2 concentration, $C_{\mathrm{L,can}}$ is canopy mean leaf internal CO_2 concentration, $D_{\mathrm{a,can}}$ is mean canopy-air vapour pressure deficit and TR is the total transpiration rate. Assuming a constant $C_{\mathrm{L,can}}/C_{\mathrm{a,can}}$ in screened and open canopies, the relative humidity in the screened plantation must be high enough (i.e., $D_{\mathrm{a,can}}$ small enough) to overcompensate for the reduction in $C_{\mathrm{a,can}}$ during daytime, despite the higher temperature. The daytime average canopy-air $C_{\mathrm{a,can}}/D_{\mathrm{a,can}}$ ratio in the screened plantation is 0.187 ppm Pa^{-1} and 0.157 ppm Pa^{-1} in the open plantation, which is about 18% smaller, demonstrating the validity of this relationship. Discrepancies between ratios of WUE in screened and open systems estimated through Eq. 23 and Table 3 can be attributed to non-uniform leaf area density and the accounting of deviations from a constant $C_{\mathrm{L,can}}/C_{\mathrm{a,can}}$.

4 Conclusions

A proposed model for flow and scalar transport inside spatially extensive screenhouses was used to explore how the bi-directional interaction between plants and their microclimate is amplified in protected environments due to the presence of a screen. In particular, model runs were conducted to address how the screen alters the mean flow field, turbulent stresses, radiative and energy fluxes, as well as scalar sources, sinks, fluxes, and mean concentration compared to their 'open' canopy state (used as a reference here). Moreover, the study addressed to what extent these alterations were induced by the screen modifications to the radiation-energy balance versus the aerodynamic effects. The model results show that the presence of a screen reduces the velocity statistics responsible for turbulent transport and the effective roughness of the surface. The radiation modulation by the screen had minor effect on sensible-heat exchanges, and most of the differences in the sensible heat between open and screenhoused plantations are in fact due to differences in the turbulent transport. The model results also show that reductions in latent-heat fluxes are consequences of both radiation and turbulent transport modulation, since those changes are related to the entire microclimate and not only to sensible heat. The CO_2 dynamics inside the screenhouse are significantly affected by both radiation and momentum exchange modulations. The presence of a screen resulted in a warmer and more humid environment inside the screenhouse, promoting reductions in both assimilation and transpiration. However, the overall effect of the screen was to enhance the water-use efficiency thereby resulting in potential water savings for the same amount of gross productivity.

Acknowledgements The authors thank Mr. U. Dicken (ARO) for providing part of the field data of the banana screenhouse and to Polysack LTD., Israel, for providing the screen sample. This study was supported by Research Grant Award No. IS-4374-11C from BARD, the United States - Israel Binational Agricultural Research and Development Fund, the United States Department of Agriculture (USDA #2011-67003-30222), and the National Science Foundation (NSF-EAR-10-13339, NSF-AGS-11-02227, and NSF-CBET-103347).

M. Siqueira acknowledges support from Conselho Nacional de Desenvolvimento Científico e Tecnológico, Brazil (CNPq # 306525/2010-0), and G. Katul also acknowledges the support from the Fulbright-Italy Distinguished Fellows program.

Appendix A: Terms in the Stress Equation (Eq. 3)

The general form of the production term, P, in Eq. 3 is given by:

$$P_{ij} = -\left(\overline{u_i' u_k'}\frac{\partial \overline{u}}{\partial x_k} + \overline{u_j' u_k'}\frac{\partial \overline{u}}{\partial x_k}\right), \tag{24}$$

and following Wilson (1988), the redistribution term, R, is parametrized by three contributions; turbulence-turbulence interaction, mean-strain-turbulence interaction and a wall-reflection term. These are, respectively, given by:

$$R_{ij,1} = -c_1\frac{\varepsilon}{k}\left(\overline{u_i' u_j'} - \frac{2}{3}k\delta_{ij}\right), \tag{25}$$

$$R_{ij,2} = -c_2\left(P_{ij} - \frac{2}{6}P_{kk}\delta_{ij}\right), \tag{26}$$

$$R'_{ij,1} = -c_1'\frac{\varepsilon}{k}\left(\overline{u_k' u_m'}n_k n_m\delta_{ij} - \frac{3}{2}\overline{u_k' u_i'}n_k n_j - \frac{3}{2}\overline{u_k' u_j'}n_k n_i\right) f\,(z), \tag{27}$$

where c_1, c_2 and c_1' are model empirical constants, n_k are components of a unit vector normal to the surface (in this case $n_k = \delta_{k3}$) and f is a wall proximity function, which, for the present case, is given by:

$$f\,(z) = \frac{k^{3/2}}{2.5\varepsilon}\left(\frac{1}{z}\right). \tag{28}$$

The transport term is given by:

$$T_{ij} = -\frac{\partial}{\partial x_k}\overline{u_i' u_j' u_k'}, \tag{29}$$

with the triple correlation parametrized as (Wilson 1988):

$$\overline{u_i' u_j' u_k'} = -c_s\frac{k}{\varepsilon}\left(\overline{u_i' u_l'}\frac{\partial \overline{u_j' u_k'}}{\partial x_l} + \overline{u_j' u_l'}\frac{\partial \overline{u_i' u_k'}}{\partial x_l} + \overline{u_k' u_l'}\frac{\partial \overline{u_i' u_j'}}{\partial x_l}\right). \tag{30}$$

For Eqs. 25 to 30, in the case considered here (planar homogeneous) only the streamwise mean-velocity component is different than zero and all derivatives, other than vertical, vanish. The values of the model constants are provided in Table 4.

Appendix B: Derivation of Screen Radiation Properties

The screen radiation properties can be obtained from the radiation budget above and below the screen (system of equations below) with the measured shortwave and longwave incoming (subscript in), outgoing (subscript out), over (subscript o) and under (subscript u) the screen (see text and Fig. 2 for experimental set-up):

$$SW_{\mathrm{in,u}} = SW_{\mathrm{in,o}}\left[\phi\left(\tau_{\mathrm{SW,b}} f_{\mathrm{SW,b}} + \tau_{\mathrm{SW,d}} f_{\mathrm{SW,d}}\right) + (1-\phi)\right] + SW_{\mathrm{out,u}}\phi\rho_{\mathrm{sc,SW}}, \quad (31)$$

$$SW_{\mathrm{out,o}} = SW_{\mathrm{out,u}}\left[\phi\tau_{\mathrm{SW,d}} + (1-\phi)\right] + SW_{\mathrm{in,o}}\phi\rho_{\mathrm{sc,SW}}, \quad (32)$$

$$LW_{\mathrm{in,u}} = LW_{\mathrm{in,o}}\left[\phi\tau_{\mathrm{LW}} + (1-\phi)\right] + LW_{\mathrm{out,u}}\phi\rho_{\mathrm{sc,LW}} + \phi e\sigma_{\mathrm{SB}} T_{\mathrm{sc}}^4, \quad (33)$$

$$LW_{\mathrm{out,o}} = LW_{\mathrm{out,u}}\left[\phi\tau_{\mathrm{LW}} + (1-\phi)\right] + LW_{\mathrm{in,o}}\phi\rho_{\mathrm{sc,LW}} + \phi e\sigma_{\mathrm{SB}} T_{\mathrm{sc}}^4, \quad (34)$$

$$\tau_{\mathrm{LW}} + \rho_{\mathrm{sc,LW}} + e = 1, \quad (35)$$

where $f_{\mathrm{SW,b}}$ and $f_{\mathrm{SW,d}}$ are ratios of the direct beam shortwave and diffuse shortwave respectively to total measured shortwave ($SW_{\mathrm{in,o}}$) such that $f_{\mathrm{SW,b}} + f_{\mathrm{SW,d}} = 1$. The split of $SW_{\mathrm{in,o}}$ between direct beam and diffuse shortwave was estimated following Goudrian and Laar (1994). Data with a zenith angle $> 60°$ were used to determine $\tau_{\mathrm{SW,d}}$, assuming that $f_{\mathrm{SW,d}} >> f_{\mathrm{SW,b}}$ for such high zenith angles. Because $\tau_{\mathrm{SW,b}}$, in contrast to $\tau_{\mathrm{SW,d}}$, may vary with zenith angle, zenith angles $< 60°$ were used to estimate $\tau_{\mathrm{SW,b}}$ as a function of zenith angle with the knowledge of $\tau_{\mathrm{SW,d}}$.

References

Baldocchi D, Meyers T (1998) On using eco-physiological, micrometeorological and biogeochemical theory to evaluate carbon dioxide, water vapor and trace gas fluxes over vegetation: a perspective. Agric For Meteorol 90(1-2):1–25

Boulard T, Baille A (1993) A simple greenhouse climate control model incorporating effects of ventilation and evaporative cooling. Agric For Meteorol 65(3-4):145–157

Boulard T, Kittas C, Roy JC, Wang S (2002) Convective and ventilation transfers in greenhouses, part 2: determination of the distributed greenhouse climate. Biosyst Eng 83(2):129–147

Campbell GS, Norman JM (1998) An introduction to environmental biophysics. Springer, New York 286

Cava D, Katul GG (2008) Spectral short-circuiting and wake production within the canopy trunk space of an alpine hardwood forest. Boundary-Layer Meteorol 126(3):415–431. doi:10.1007/s10546-007-9246-x

Cohen S, Fuchs M (1999) Measuring and predicting radiometric properties of reflective shade nets and thermal screens. J Agric Eng Res 73(3):245–255

Daly E, Porporato A, Rodriguez-Iturbe I (2004) Coupled dynamics of photosynthesis, transpiration, and soil water balance. Part i: upscaling from hourly to daily level. J Hydrometeorol 5(3):546–558

FAO (2011) The state of the world's land and water resources for food and agriculture (SOLAW). FAO, Rome, pp 12. http://www.fao.org/docrep/meeting/022/mb213e.pdf

Farquhar GD, Caemmerer SV, Berry JA (1980) A biochemical-model of photosynthetic CO_2 assimilation in leaves of c-3 species. Planta 149(1):78–90

Fay P, Kelley A, Procter A, Hui D, Jin V, Jackson R, Johnson H, Polley H (2009) Primary productivity and water balance of grassland vegetation on three soils in a continuous CO_2 gradient: Initial results from the lysimeter CO_2 gradient experiment. Ecosystems 12(5):699–714

Finnigan J (2000) Turbulence in plant canopies. Annu Rev Fluid Mech 32:519–571. doi:10.1146/annurev.fluid.32.1.519

Gibson MM, Rodi W (1981) A Reynolds-stress closure-model of turbulence applied to the calculation of a highly curved mixing layer. J Fluid Mech 103(FEB):161–182

Goudrian J, Laar HHv (1994) Modelling potencial crop growth processes. Kluwer, Dordrecht 256

Hanjalic K, Launder BE (1972) Reynolds stress model for turbulence and its application to thin shear flows. J Fluid Mech 52(4):609–638

Hsieh CI, Katul G (2009) The Lagrangian stochastic model for estimating footprint and water vapor fluxes over inhomogeneous surfaces. Int J Biometeorol 53(1):87–100. doi:10.1007/s00484-008-0193-0

Incropera FA, Witt DPD (1996) Introduction to heat transfer, 3rd edn. Wiley, New York 912

Juang JY, Katul GG, Siqueira MB, Stoy PC, McCarthy HR (2008) Investigating a hierarchy of Eulerian closure models for scalar transfer inside forested canopies. Boundary-Layer Meteorol 128(1):1–32

Katul GG, Chang WH (1999) Principal length scales in second-order closure models for canopy turbulence. J Appl Meteorol 38(11):1631–1643

Katul GG, Mahrt L, Poggi D, Sanz C (2004) One- and two-equation models for canopy turbulence. Boundary-Layer Meteorol 113(1):81–109

Katul GG, Palmroth S, Oren R (2009) Leaf stomatal responses to vapour pressure deficit under current and CO_2-enriched atmosphere explained by the economics of gas exchange. Plant Cell Environ 32(8):968–979. doi:10.1111/j.1365-3040.2009.01977.x

Katul G, Manzoni S, Palmroth S, Oren R (2010) A stomatal optimization theory to describe the effects of atmospheric CO_2 on leaf photosynthesis and transpiration. Ann Bot 105(3):431–442. doi:10.1093/aob/mcp292

Kindelan M (1980) Dynamic modeling of greenhouse environment. Trans ASAE 23(5):1232–1239

Lai CT, Katul G, Butnor J, Siqueira M, Ellsworth D, Maier C, Johnsen K, McKeand S, Oren R (2002) Modelling the limits on the response of net carbon exchange to fertilization in a south-eastern pine forest. Plant Cell Environ 25(9):1095–1119

Leuning R (1995) A critical-appraisal of a combined stomatal-photosynthesis model for C-3 plants. Plant Cell Environ 18(4):339–355

Leuning R, Kelliher FM, Depury DGG, Schulze ED (1995) Leaf nitrogen, photosynthesis, conductance and transpiration—scaling from leaves to canopies. Plant Cell Environ 18(10):1183–1200

Majdoubi H, Boulard T, Fatnassi H, Bouirden L (2009) Airflow and microclimate patterns in a one-hectare canary type greenhouse: An experimental and CFD assisted study. Agric For Meteorol 149(6-7):1050–1062

Manzoni S, Katul G, Fay PA, Polley HW, Porporato A (2011) Modeling the vegetation-atmosphere carbon dioxide and water vapor interactions along a controlled CO_2 gradient. Ecol Model 222(3):653–665. doi:10.1016/j.ecolmodel.2010.10.016

Meyers TP, Paw UKTP (1987) Modeling the plant canopy micrometeorology with higher-order closure principles. Agric For Meteorol 41(1-2):143–163

Poggi D, Katul GG (2006) Two-dimensional scalar spectra in the deeper layers of a dense and uniform model canopy. Boundary-Layer Meteorol 121(2):267–281. doi:10.1007/s10546-006-9075-3

Poggi D, Katul GG, Albertson JD (2004a) Momentum transfer and turbulent kinetic energy budgets within a dense model canopy. Boundary-Layer Meteorol 111(3):589–614

Poggi D, Porporato A, Ridolfi L, Albertson JD, Katul GG (2004b) The effect of vegetation density on canopy sub-layer turbulence. Boundary-Layer Meteorol 111(3):565–587

Poggi D, Katul GG, Cassiani M (2008) On the anomalous behavior of the Lagrangian structure function similarity constant inside dense canopies. Atmos Environ 42(18):4212–4231. doi:10.1016/j.atmosenv.2008.01.020

Raupach MR (1989) A practical Lagrangian method for relating scalar concentrations to source distributions in vegetation canopies. Q J Roy Meteorol Soc 115(487):609–632. doi:10.1002/qj.49711548710

Raupach MR, Shaw RH (1982) Averaging procedures for flow within vegetation canopies. Boundary-Layer Meteorol 22(1):79–90

Roy JC, Boulard T, Kittas C, Wang S (2002) Convective and ventilation transfers in greenhouses. Part 1: the greenhouse considered as a perfectly stirred tank. Biosyst Eng 83(1):1–20

Sanz C (2003) A note on k-epsilon modelling of vegetation canopy air-flows. Boundary-Layer Meteorol 108(1):191–197

Singh G, Singh PP, Lubana PPS, Singh KG (2006) Formulation and validation of a mathematical model of the microclimate of a greenhouse. Renew Energy 31(10):1541–1560

Siqueira M, Lai CT, Katul G (2000) Estimating scalar sources, sinks, and fluxes in a forest canopy using Lagrangian, Eulerian, and hybrid inverse models. J Geophys Res-Atmos 105(D24):29475–29488. doi:10.1029/2000jd900543

Siqueira MB, Katul GG, Sampson DA, Stoy PC, Juang JY, McCarthy HR, Oren R (2006) Multiscale model intercomparisons of CO_2 and H_2O exchange rates in a maturing southeastern us pine forest. Glob Chang Biol 12(7):1189–1207

Soribe FI, Curry RB (1973) Simulation of lettuce growth in an air-supported plastic greenhouse. J Agric Eng Res 18(2):133–140

Tanny J, Cohen S (2003) The effect of a small shade net on the properties of wind and selected boundary layer parameters above and within a citrus orchard. Biosyst Eng 84(1):57–67. doi:10.1016/s1537-5110(02)00233-7

Tanny J, Liu HJ, Cohen S (2006) Airflow characteristics, energy balance and eddy covariance measurements in a banana screenhouse. Agric For Meteorol 139(1-2):105–118. doi:10.1016/j.agrformet.2006.06.004

Tanny J, Moller M, Cohen S (2009) Aerodynamic properties of boundary layers along screens. Biosyst Eng 102(2):171–179. doi:10.1016/j.biosystemseng.2008.11.015

Tanny J, Dicken U, Cohen S (2010) Vertical variation in turbulence statistics and energy balance in a banana screenhouse. Biosyst Eng 106(2):175–187. doi:10.1016/j.biosystemseng.2010.03.008

Teitel M, Atias M, Barak M (2010) Gradients of temperature, humidity and CO_2 along a fan-ventilated greenhouse. Biosyst Eng 106(2):166–174

Thom AS (1971) Momentum absorption by vegetation. Q J Roy Meteorol Soc 97:414–428
Turner DW, Fortescue JA, Thomas DS (2007) Environmental physiology of the bananas (*musa* spp.). Braz J Plant Physiol 19(4):463–484
Tuzet A, Perrier A, Leuning R (2003) A coupled model of stomatal conductance, photosynthesis and transpiration. Plant Cell Environ 26(7):1097–1116
Wang YP, Leuning R (1998) A two-leaf model for canopy conductance, photosynthesis and partitioning of available energy i: Model description and comparison with a multi-layered model. Agric For Meteorol 91(1-2):89–111
Willits DH (2003) Cooling fan-ventilated greenhouses: a modelling study. Biosyst Eng 84(3):315–329
Wilson JD (1988) A 2nd-order closure model for flow through vegetation. Boundary-Layer Meteorol 42(4):371–392
Yang X, Short TH, Fox RD, Bauerle WL (1990) Dynamic modeling of the microclimate of a greenhouse cucumber row-crop. 1. theoretical-model. Trans ASAE 33(5):1701–1709